AMERICAN SOCIETY FOR MICROBIOLOGY | Applied and Environmental Microbiology®

Proteome Response of a Metabolically Flexible Anoxygenic Phototroph to Fe(II) Oxidation

Casey Bryce,[a] Mirita Franz-Wachtel,[b] Nicolas C. Nalpas,[b] Jennyfer Miot,[c] Karim Benzerara,[c] James M. Byrne,[a] Sara Kleindienst,[a,d] Boris Macek,[b] Andreas Kappler[a]

[a]Geomicrobiology, University of Tübingen, Tübingen, Germany
[b]Proteome Center Tübingen, University of Tübingen, Tübingen, Germany
[c]Sorbonne Université, MNHN, UMR 7590 CNRS, Institut de Minéralogie, Physique des Matériaux et de Cosmochimie, IMPMC, Paris, France
[d]Microbial Ecology, University of Tübingen, Tübingen, Germany

ABSTRACT The oxidation of Fe(II) by anoxygenic photosynthetic bacteria was likely a key contributor to Earth's biosphere prior to the evolution of oxygenic photosynthesis and is still found in a diverse range of modern environments. All known phototrophic Fe(II) oxidizers can utilize a wide range of substrates, thus making them very metabolically flexible. However, the underlying adaptations required to oxidize Fe(II), a potential stressor, are not completely understood. We used a combination of quantitative proteomics and cryogenic transmission electron microscopy (cryo-TEM) to compare cells of *Rhodopseudomonas palustris* TIE-1 grown photoautotrophically with Fe(II) or H_2 and photoheterotrophically with acetate. We observed unique proteome profiles for each condition, with differences primarily driven by carbon source. However, these differences were not related to carbon fixation but to growth and light harvesting processes, such as pigment synthesis. Cryo-TEM showed stunted development of photosynthetic membranes in photoautotrophic cultures. Growth on Fe(II) was characterized by a response typical of iron homeostasis, which included an increased abundance of proteins required for metal efflux (particularly copper) and decreased abundance of iron import proteins, including siderophore receptors, with no evidence of further stressors, such as oxidative damage. This study suggests that the main challenge facing anoxygenic phototrophic Fe(II) oxidizers comes from growth limitations imposed by autotrophy, and, once this challenge is overcome, iron stress can be mitigated using iron management mechanisms common to diverse bacteria (e.g., by control of iron influx and efflux).

IMPORTANCE The cycling of iron between redox states leads to the precipitation and dissolution of minerals, which can in turn impact other major biogeochemical cycles, such as those of carbon, nitrogen, phosphorus and sulfur. Anoxygenic phototrophs are one of the few drivers of Fe(II) oxidation in anoxic environments and are thought to contribute significantly to iron cycling in both modern and ancient environments. These organisms thrive at high Fe(II) concentrations, yet the adaptations required to tolerate the stresses associated with this are unclear. Despite the general consensus that high Fe(II) concentrations pose numerous stresses on these organisms, our study of the large-scale proteome response of a model anoxygenic phototroph to Fe(II) oxidation demonstrates that common iron homeostasis strategies are adequate to manage this. The bulk of the proteome response is not driven by adaptations to Fe(II) stress but to adaptations required to utilize an inorganic carbon source. Such a global overview of the adaptation of these organisms to Fe(II) oxidation provides valuable insights into the physiology of these biogeochemically important organisms and suggests that Fe(II) oxidation may not pose as many challenges to anoxygenic phototrophs as previously thought.

Received 15 May 2018 **Accepted** 7 June 2018
Accepted manuscript posted online 18 June 2018
Citation Bryce C, Franz-Wachtel M, Nalpas NC, Miot J, Benzerara K, Byrne JM, Kleindienst S, Macek B, Kappler A. 2018. Proteome response of a metabolically flexible anoxygenic phototroph to Fe(II) oxidation. Appl Environ Microbiol 84:e01166-18. https://doi.org/10.1128/AEM.01166-18.
Editor Volker Müller, Goethe University Frankfurt am Main

Address correspondence to Casey Bryce, casey.bryce@uni-tuebingen.de.

KEYWORDS phototrophic iron oxidation, iron stress, anoxygenic photosynthesis, proteomics, cryogenic electron microscopy

Anoxygenic phototrophic Fe(II) oxidizers fix CO_2 by oxidation of Fe(II) (equation 1 [+ *hv* indicates that the reaction is light dependent]).

$$HCO_3^- + 4Fe^{2+} + 10H_2O + h\nu \rightarrow (CH_2O) + 4Fe(OH)_3 + 7H^+ \quad (1)$$

This process is thought to have fueled the Earth's biosphere prior to the evolution of oxygenic photosynthesis and is likely to have been a key contributor in the deposition of vast formations of layered Fe(II)-Fe(III) and Si-rich rock during Earth's early history (1–3). Organisms capable of this metabolism are still found in many modern environments, including Fe(II)-rich (4–7) and Fe(II)-poor (8) stratified lakes, as well as both freshwater (9, 10) and marine sediments (11–14). These microorganisms belong to the purple sulfur bacteria (*Gammaproteobacteria*), purple nonsulfur bacteria (*Alphaproteobacteria*), and green sulfur bacteria (*Chlorobi*).

Anoxygenic phototrophs show remarkable versatility with regard to their metabolism. They can fix CO_2 using Fe(II), H_2, or H_2S as an electron donor (photoautotrophy), or they can use organic compounds as a carbon source (photoheterotrophy) (9, 10, 12, 14, 15). Some isolates can also grow chemoheterotrophically with dioxygen without any light at all, e.g., *Rhodopseudomonas palustris* TIE-1 (Jiao et al. [9]). Not only can these organisms switch metabolisms, but they can also use multiple metabolisms simultaneously. Previous studies with purple nonsulfur bacteria have shown that Fe(II) and H_2 can be utilized simultaneously, although this led to a lower rate of Fe(II) oxidation than that with Fe(II) alone (16). The simultaneous use of organic carbon and CO_2 fixation with Fe(II) as an electron donor has also been observed and depends on the identity of the carbon source. For example, *Rhodopseudomonas palustris* strain TIE-1 utilizes Fe(II) and lactate simultaneously but preferentially utilizes acetate before commencing Fe(II) oxidation (17). The cellular processes which facilitate this metabolic flexibility are not well constrained. For example, the proteins responsible for Fe(II) oxidation itself have only been determined in two anoxygenic phototrophic Fe(II) oxidizers (*Rhodopseudomonas palustris* TIE-1 and *Rhodobacter ferrooxidans* SW2) (18–21). However, the proteins identified are different even between these two purple nonsulfur bacteria and cannot be used as general markers for active Fe(II) oxidation.

Metabolic flexibility is clearly beneficial in soils, sediments, and aquatic habitats where anoxygenic phototrophs are found, as redox conditions and substrate availability can continuously fluctuate due to changes in light conditions (thus oxygen production), precipitation, physical disturbance, or competition with other organisms or abiotic reactions. Physical mixing of sediments, e.g., by wave action or bioturbation, can also act to redistribute organisms within the sediment column such that they are outside their favored redox zone. This has been shown to occur with Fe(II)-oxidizing bacteria in marine sediments where the bacteria are found to be equally abundant at all sediment depths regardless of redox or substrate conditions (11). Metabolic flexibility is a powerful strategy for coping with such varied environmental conditions, as these organisms increase their chances of being able to proliferate in any environment to which they are exposed.

Of all of the potential metabolisms these bacteria could use, Fe(II) oxidation would appear to pose the most challenges. First, they must be able to avoid encrustation of their outer membranes by Fe(III) minerals which form during Fe(II) oxidation (22, 23). Furthermore, they may also have to compete with Fe(III) minerals for trace nutrients which readily sorb to mineral surfaces (24). High iron concentrations may also induce stress on the cells. A growing body of literature suggests that iron can be harmful even under an anoxic atmosphere (25–28), despite the lack of oxygen radicals produced via the Fenton reaction which drives iron toxicity in oxic environments (29). So far, stress resulting from high Fe(II) concentrations under anoxic conditions has been suggested to be related to the formation of organic radicals, such as glutathione radicals,

which subsequently transfer electrons to cellular biopolymers (28) and to oxygen-independent photochemical reactions with Fe minerals, which can abiotically produce reactive oxygen species (30, 31). The process of Fe(II) oxidation itself has even been proposed as a defense mechanism against the stressful effects of high concentrations of Fe(II) (25). For example, the highest Fe(II) oxidation rates are observed when *Rhodopseudomonas palustris* TIE-1 cells are precultured on Fe(II) (18), suggesting that, whatever the cause, an adaptive response to Fe(II) stress is required.

If we are to better understand how these important organisms adapt to all of the challenges associated with metabolic flexibility and high Fe(II) concentrations in particular, it is essential to take a holistic view of Fe(II) oxidation. In order to construct an overall impression of the adaptations anoxygenic phototrophs require to conduct Fe(II) oxidation, we have adopted a shotgun quantitative proteomics approach with the goal to analyze, on a large scale, the protein complement of a model anoxygenic phototroph, *Rhodopseudomonas palustris* TIE-1, grown with either Fe(II) (10 mM), H_2 (80:20 H_2/CO_2), or acetate (10 mM). Large-scale analysis of the proteins comprising these cells provides a snapshot of the processes which are active under that condition, as opposed to transcriptome analysis, which does not account for any posttranscriptional regulation. By combining this technique with visual comparisons of the cells using cryogenic transmission electron microscopy (cryo-TEM), we can gain a detailed overview of how the cells adapt to different substrate conditions. *Rhodopseudomonas palustris* TIE-1, a purple nonsulfur bacterium, is arguably the best-studied Fe(II)-oxidizing isolate available (9, 18, 26, 32, 33). The entire genome has been sequenced and is essential for extracting meaningful functional insights from proteomics data, and the mechanism for iron oxidation is well constrained, making TIE-1 an excellent model for our study.

RESULTS

Global overview of proteomes in *Rhodopseudomonas palustris* TIE-1 cultures grown with different substrates. In order to gain a holistic overview of the cellular processes which facilitate Fe(II) oxidation in *Rhodopseudomonas palustris* TIE-1, we compared the proteomes of cells from parallel cultures grown with Fe(II), H_2, and acetate. The time taken before the cultures reached the mid-exponential phase, and thus the point of cell harvest, was substrate dependent. Photoheterotrophic cultures (grown on acetate) grew quickly and reached the mid-exponential phase after 18 h. Photoautotrophic cultures [grown on Fe(II) or H_2] grew more slowly, with the iron-grown cultures reaching the mid-exponential phase after 140 h and with H_2-grown cultures after 257 h.

Following protein extraction, mass spectrometry analysis, and subsequent downstream processing, 2,049 protein groups were identified across all substrates, with a false discovery rate of 0.01. Overall, there was very good reproducibility between triplicates (as seen in Fig. 1A, with average correlation $>$95%). High similarity was observed between both photoautotrophic cultures, i.e., those grown with Fe(II) or H_2 (average correlation, 83%; clustering shown in Fig. 1B). Cells grown with Fe(II) had an average correlation of 63% compared to cells grown with acetate, and those with H_2 had an average correlation of 73%. In a comparison of proteins which show significantly different expression when grown on Fe(II) (significance criteria outlined in Materials and Methods), we identified 445 proteins which showed higher expression than in acetate-grown cells and 189 proteins which showed higher expression than in hydrogen-grown cells. Fe(II)-grown cells had 241 proteins which were significantly lower in abundance than in acetate-grown cells and 164 proteins lower in abundance than in hydrogen-grown cells. Hydrogen-grown cells had 361 proteins with higher expression and 212 proteins with lower expression than in those grown with acetate. Many proteins were significantly more abundant in both Fe(II)- and H_2-grown cells than in those grown with acetate; similarly, many proteins were also lower in abundance in both Fe(II)- and H_2-grown cells than in those grown with acetate (Fig. 2). The similarities between both autotrophic cultures is reflected in the large number of proteins which were only

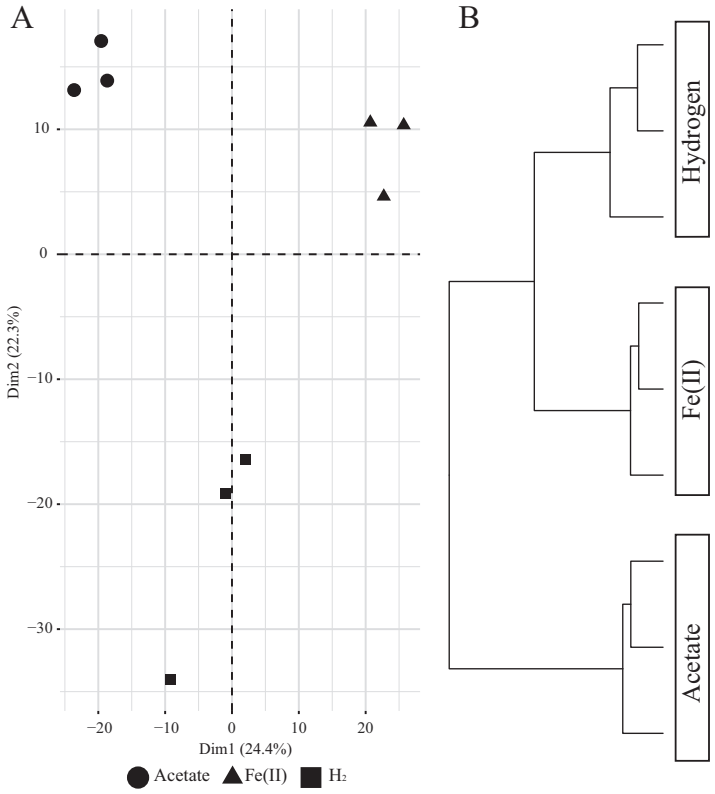

FIG 1 (A) Principal component analysis (PCA) of all protein group abundances for all three growth conditions. (B) Hierarchical clustering shows higher similarities between photoautotrophic cells than with photoheterotrophic cells. The average Spearman correlation between triplicates was >95%. The average Spearman correlation between Fe(II) and H_2 was 83%, compared to 73% between H_2 and acetate and 63% between Fe(II) and acetate. Dim1 and Dim2 represent the two dimensions of the principal component analysis.

quantified under H_2- and Fe(II)-grown conditions (Fig. 2) and not under the acetate-grown conditions (Fig. 2).

Commonalities and differences between autotrophic and heterotrophic metabolisms. The main factor driving the differences between conditions was the carbon source, i.e., organic carbon as acetate and inorganic carbon as CO_2 (Fig. 2). Therefore, if we want to better understand the adaptations required for Fe(II) oxidation, we need to first understand the adaptation to an organic or inorganic carbon source. To determine which proteins are important specifically for autotrophic metabolism, we identified proteins which were significantly higher in abundance under both the Fe(II)

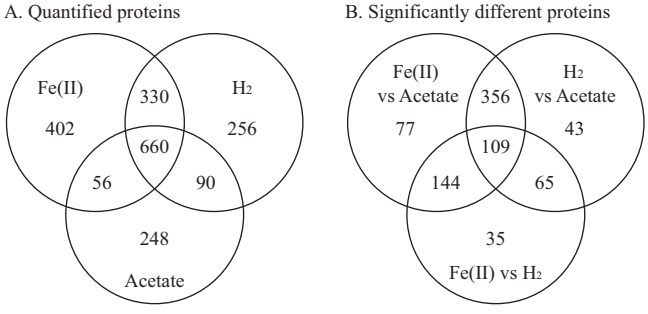

FIG 2 Venn diagram showing number of proteins quantified under each condition (A) and significantly different in abundance (B) in each of the three comparison groups. In total, 1,448 proteins were quantified with Fe(II), 1,336 proteins were quantified with H_2, and 1,054 proteins were quantified with acetate.

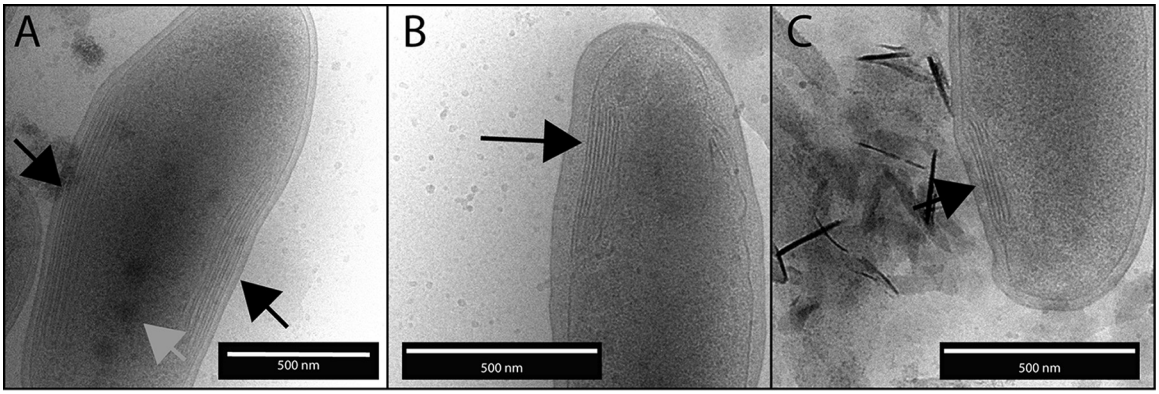

FIG 3 Cryo-transmission electron micrographs of *Rhodopseudomonas palustris* TIE-1 cells grown with acetate (A), H_2 (B), and Fe(II) (C) showing the differences in the lengths of intracytoplasmic membranes. Black arrows point to the positions of intracellular cytoplasmic membranes. Gray arrow points to intracellular polyphosphates which are not unique to any one condition.

and H_2 conditions than under the acetate conditions (258 proteins; see Data Set S1 in the supplemental material). These include proteins for a diverse range of functions, including energy and electron transport processes, amino acid synthesis, and motility. PioA, thought to be the iron oxidase in *Rhodopseudomonas palustris* TIE-1 (18), was significantly higher in both Fe(II)-grown and hydrogen-grown than in acetate-grown cells (adjusted $P = 2.1 \times 10^{-6}$ and 2.7×10^{-6}, respectively), as was PioB, a membrane porin thought to anchor PioA in the outer membrane [adjusted $P = 0.003$ in Fe(II) versus acetate and 0.005 in H_2 versus acetate]. PioC, a high-potential iron-sulfur protein associated with the oxidation of Fe(II) (33), was not significantly different in abundance between any condition [i.e., Fe(II) versus acetate, Fe(II) versus H_2, or H_2 versus acetate].

There were 98 proteins significantly lower in abundance under both autotrophic conditions [i.e., lower in both Fe(II) and H_2 than in acetate; Data Set S2]. These were primarily general housekeeping proteins, including those for protein synthesis. Gene set enrichment analysis showed significant enrichment of ribosomal proteins in acetate-grown cells relative to those grown with H_2 or Fe(II) (data not shown). We also observed a significantly lower abundance of the following 4 proteins related to pigment synthesis: BchB and BchN for light-independent chlorophyll synthesis, 1 protein related to bacteriochlorophyll synthesis (Rpal_1711), and a geranylgeranyl reductase involved in chlorophyll biosynthesis (Rpal_1721). A putative photosynthetic complex assembly protein (Rpal_1737) was also lower in abundance under both the Fe(II) and hydrogen conditions than under acetate conditions.

In *Rhodopseudomonas palustris* TIE-1, much of the light-harvesting machinery is located on long folded intracytoplasmic membranes. Therefore, we used cryo-TEM to assess if the differences in the expression of proteins for pigments in the photoautotrophic compared to the photoheterotrophic conditions was manifested in differences in these membranes. Cells grown with acetate have long thick intracellular cytoplasmic membranes which occupy, on average, 113 μm^2 (standard deviation [SD], 38 μm^2, $n = 16$; including the intramembrane space), which are observed on both sides of the cell in 50% of the acetate-grown cells imaged (Fig. 3). In contrast, cells grown with H_2 or Fe(II) show that the intracytoplasmic membranes are limited to smaller regions within the cell [for H_2, 22 μm^2; SD, 18 μm^2, $n = 33$; for Fe(II), 19 μm^2; SD, 16 μm^2, $n = 19$]. Only 11% of the Fe(II)-grown cells and 9% of the H_2-grown cells imaged had membranes on both sides. No acetate cell was imaged without visible membranes, whereas 26% of the Fe(II) cells imaged had no visible membranes, as did 21% of hydrogen-grown cells (Fig. 3). No differences in the lengths of the cells were observed under any condition, and there is no clear difference observable by cryo-TEM between the H_2 and Fe(II) growth conditions. Intracellular round electron-dense polyphosphates were observed under all growth conditions but not necessarily in all cells observed (most clearly seen in Fig. 3A).

TABLE 1 Selection of proteins of interest with significantly higher abundance in Fe(II) than in both H_2 and acetate, indicating that they are important for adaptation to Fe(II) oxidation[a]

				Fe(II) vs acetate		Fe(II) vs H_2		
Protein by functional group	Description[b]	Gene	Locus tag	log FC	adj. *P* value	log FC	adj. *P* value	Unique Fe(II)
Efflux								
B3Q633	Efflux pump membrane transporter		Rpal_0100	1.61	1.1E−02	1.53	1.3E−02	+
B3QBE5	Porin		Rpal_0539	0.37	1.7E−03	0.39	1.3E−03	
B3Q656	Efflux transporter, RND family, MFP subunit		Rpal_1604	1.23	5.8E−03	1.25	5.4E−03	+
B3QHF9	Efflux transporter, RND family, MFP subunit		Rpal_4297	0.50	2.3E−03	0.32	2.0E−02	
B3Q940	Heavy-metal efflux pump	*czcA*	Rpal_4972	2.17	3.6E−05	1.71	1.4E−04	+
Membrane processes								
B3QEG5	3-hydroxyacyl-CoA dehydrogenase NAD binding		Rpal_0887	1.81	1.5E−03	1.06	2.1E−02	
B3QCT3	Phosphatidylserine decarboxylase proenzyme	*psd*	Rpal_2217	1.30	5.3E−03	1.37	4.0E−03	+
B3Q7L0	Lipoprotein-releasing system ATP-binding protein LolD	*lolD*	Rpal_3274	0.12	1.4E−03	0.13	9.1E−04	
B3QD34	Polysaccharide export protein		Rpal_3782	0.94	1.7E−04	0.68	9.6E−04	
B3QFN0	UDP-*N*-acetylmuramate–L-alanine ligase	*murC*	Rpal_4047	0.93	8.7E−03	1.32	1.5E−03	+
B3QJ20	Uncharacterized protein		Rpal_4480	1.17	7.9E−05	1.24	5.6E−05	
B3QDE6	Polysaccharide export protein		Rpal_5320	0.33	5.1E−03	0.26	1.5E−02	
Motility								
B3Q871	Putative methyl-accepting chemotaxis sensory transducer		Rpal_0260	0.24	9.0E−04	0.27	4.8E−04	
B3QF47	Methyl-accepting chemotaxis sensory transducer		Rpal_0924	1.56	1.0E−02	1.81	5.2E−03	+
B3QIZ3	Uncharacterized protein		Rpal_4453	1.07	2.6E−02	1.00	3.4E−02	+
B3QIZ5	Flagellar basal body protein		Rpal_4455	0.37	2.2E−03	0.25	1.6E−02	
B3QKS6	Methyl-accepting chemotaxis sensory transducer		Rpal_4682	1.08	2.6E−02	1.25	1.4E−02	+
Energy metabolism								
B3QK17	Cytochrome *c* oxidase, cbb_3 type, subunit II		Rpal_0019	0.26	3.2E−02	0.30	1.8E−02	
B3Q748	ATP synthase subunit delta	*atpH*	Rpal_0174	0.35	3.4E−05	0.34	3.6E−05	
B3QF34	ATP synthase subunit-b1	*atpF1*	Rpal_0911	0.30	2.4E−05	0.30	2.2E−05	
B3QIK1	Cytochrome *b*		Rpal_1385	0.27	2.2E−02	0.42	2.6E−03	
B3Q7B0	Photosynthetic reaction center L subunit		Rpal_1716	0.89	2.0E−03	0.82	3.1E−03	
B3Q7B1	Reaction center protein M chain		Rpal_1717	0.51	2.8E−04	0.55	1.8E−04	
A5YN36	Cytochrome *c* class I (cytochrome c_2)	*cycA*	Rpal_1724	0.18	3.4E−02	0.19	2.7E−02	
B3QH56	Cytochrome B561		Rpal_2736	0.31	1.0E−02	0.44	1.6E−03	
B3QJL2	K^+-insensitive pyrophosphate-energized proton pump	*hppA*	Rpal_3012	0.93	2.4E−02	1.04	1.5E−02	

[a]For each comparison, log FC is the log 10-fold change between Fe(II) and the condition of interest; adj. *P* value is the adjusted *P* value for the Tukey test. Column "Unique Fe(II)" indicates which proteins, in addition to being significantly higher under the Fe(II) condition relative to both H_2 and acetate conditions, were detected only under the conditions with Fe(II). Proteins are grouped broadly into functional groups.
[b]MFP, membrane fusion protein; CoA, coenzyme A.

Given that one of the primary differences between the acetate and H_2/Fe(II) conditions (i.e., photoheterotrophy versus photoautotrophy) was the carbon source, we mapped protein expression onto the KEGG pathway for "carbon fixation in photosynthetic organisms" (Fig. S1). This showed no clear increase in abundance of proteins of this pathway despite the fact that many were detected, even under heterotrophic conditions. Similarly, overrepresentation analysis for KEGG orthology (KO) did not show any significant overrepresentation of carbon fixation in photoautotrophic cultures, i.e., when Fe(II) or H_2 was compared to acetate.

Proteins differing in abundance with Fe(II). We confidently identified 92 proteins which were significantly higher in abundance under Fe(II) conditions than under both H_2- and acetate-grown conditions, and 52 proteins which were significantly lower. Lists of selected proteins of interest are found in Tables 1 and 2, and a complete list can be found in Data Sets S3 and S4. Among the proteins with higher abundance are those related to motility, including those for pilus and flagellar formation and for chemotaxis. Metal efflux proteins were also highly abundant under this growth condition with Fe(II)

TABLE 2 Selection of proteins of interest with significantly lower abundance in Fe(II) than in both H_2 and acetate, indicating that they are important for adaptation to Fe(II) oxidation

Protein by functional group	Description[a]	Gene	Locus tag	Fe(II) vs acetate		Fe(II) vs H_2	
				log FC	adj. *P* value	log FC	adj. *P* value
Iron							
B3QAC8	Ferric uptake regulation protein	*fur*	Rpal_0454	−0.37	5.7E−03	−0.48	1.5E−03
B3Q8I1	Hemerythrin HHE cation binding domain protein		Rpal_1855	−0.47	1.3E−03	−0.50	9.1E−04
B3QEK7	Hemin import ATP-binding protein HmuV	*hmuV*	Rpal_2409	−0.33	2.4E−02	−0.48	4.4E−03
B3QKE1	TonB-dependent siderophore receptor		Rpal_3084	−1.43	1.1E−03	−1.07	5.0E−03
B3QEV8	TonB system transport protein ExbD		Rpal_3966	−0.94	3.9E−05	−1.00	2.7E−05
B3QB63	FeoA family protein		Rpal_5117	−1.10	2.2E−04	−1.25	1.1E−04
Photosynthesis							
B3Q7A8	Antenna complex alpha/beta-subunit		Rpal_1714	−1.72	4.9E−04	−1.17	3.8E−03
B3Q7D2	Photosynthetic complex assembly protein		Rpal_1738	−0.89	1.0E−03	−0.76	2.3E−03
B3Q6E4	Mg-protoporphyrin IX chelatase		Rpal_1693	−0.32	4.6E−03	−0.20	4.2E−02
Ribosome							
B3Q725	50S ribosomal protein L21	*rplU*	Rpal_0151	−1.89	1.3E−04	−1.54	4.3E−04
B3Q856	30S ribosomal protein S16	*rpsP*	Rpal_0245	−1.21	2.4E−04	−0.91	1.1E−03
B3Q7H1	30S ribosomal protein S4	*rpsD*	Rpal_1777	−1.58	3.1E−05	−1.21	1.4E−04
B3QBW3	30S ribosomal protein S5	*rpsE*	Rpal_3650	−1.19	6.4E−04	−0.87	3.3E−03
B3QBW4	50S ribosomal protein L18	*rplR*	Rpal_3651	−0.74	2.7E−03	−0.42	3.6E−02
B3QBW5	50S ribosomal protein L6	*rplF*	Rpal_3652	−1.12	2.1E−04	−0.80	1.3E−03
B3QBX1	30S ribosomal protein S17	*rpsQ*	Rpal_3658	−1.08	7.9E−04	−0.67	8.9E−03
B3QBX7	50S ribosomal protein L2	*rplB*	Rpal_3664	−1.33	1.7E−03	−0.75	2.7E−02
B3QC01	50S ribosomal protein L7/L12	*rplL*	Rpal_3688	−0.46	5.9E−04	−0.28	7.6E−03
B3QGL2	Translation initiation factor IF-1	*infA*	Rpal_4193	−0.38	2.4E−03	−0.21	3.9E−02

[a]For each comparison, log FC is the log 10-fold change between Fe(II) and the condition of interest; adj. *P* value is the adjusted *P* value for the Tukey test. Proteins are grouped broadly into functional groups.

as an electron donor relative to both other conditions, including two resistance-nodulation-division (RND) family efflux transporter subunits (Rpal_1604 and Rpal_4297), a CzcA family heavy-metal efflux pump (Rpal_4972), and an efflux pump membrane transporter (Rpal_0100). These are accompanied by proteins associated with processes in the outer membrane (Table 1), such as membrane biogenesis (Rpal_4047) and export of polysaccharides (Rpal_3782 and Rpal_5320). Also increased in abundance are proteins involved in the respiratory electron transport chain, including a number of cytochromes, ATP synthases, and reaction center proteins (Table 1).

Of the 52 proteins which are significantly lower in Fe(II) than in both hydrogen and acetate, many are related to iron uptake. Decreased abundance of Fur, the global negative regulator of iron uptake, is observed in the Fe(II)-grown cells, as well as decreased abundance of a TonB-dependent siderophore receptor and TonB system transport protein ExbD. FeoA, an iron uptake protein, and hemin import ATP-binding protein HmuV, as well as 10 proteins annotated as ribosome constituents, are also lower with Fe(II) than under both other conditions. Some key proteins showing lower abundance in Fe(II)-grown cells than under both other conditions are displayed in Table 2.

DISCUSSION

Physiology of TIE-1 under photoautotrophic and photoheterotrophic conditions. Our results show that distinctive proteome profiles are obtained under different substrate conditions and that the main factor driving the difference between the conditions is the carbon source. However, we see few significant differences in the abundance of carbon fixation proteins between heterotrophically and autotrophically grown cells. During photoheterotrophic growth on acetate, which is slightly less reduced than average biomass molecules, the partial oxidation of some acetate to generate electrons for biosynthesis produces more reduced redox cofactors than can be used for these biosynthetic processes, which leads to a redox imbalance inside the cell. It is known that in *Rhodopseudomonas palustris*, CO_2 fixation pathways are used to

reoxidize these cofactors and play an essential role in recycling excess electrons (34, 35). Our observation that carbon fixation pathways are expressed when acetate is provided as a carbon source are consistent with the use of carbon fixation to balance intracellular redox conditions during photoheterotrophic growth.

Differences in proteome profiles appear instead to be more generally related to the effect of organic carbon substrates on growth. Microbial growth under photoautotrophic conditions is much slower than that with acetate [with H_2-grown cultures reaching mid-exponential phase after 10 days and Fe(II)-grown cultures after 6 days, compared to less than 1 day with acetate]. Acetate-grown cells also appear to be able to divert more resources toward light harvesting. This is evidenced by the extensive intracytoplasmic photosynthetic membranes observed in acetate-grown cells using cryo-TEM and in the higher abundance of proteins for pigment synthesis. Photoautotrophic cells, however, show short spatially limited intracytoplasmic membranes (Fig. 3). It is known that anoxygenic phototrophs expand the area dedicated to intracellular cytoplasmic membranes in response to low light levels and oxygen tension (36, 37). Our results suggest that carbon source also has an important role to play in the formation of these light-harvesting membranes.

Specific adaptations of *Rhodopseudomonas palustris* TIE-1 to growth with Fe^{2+}. Expression profiles of the Fe(II)-grown Fe(II)-oxidizing cultures are characterized by control over the influx and efflux of metal ions into the cell. Numerous metal efflux proteins are highly abundant during growth on Fe(II). One of these is a copper efflux protein, an effect also observed by Bird et al. (26) when documenting the transcriptional response of acetate-grown *Rhodopseudomonas palustris* TIE-1 cells to sudden Fe(II) shock. In that study, Bird et al. demonstrated that Fe(II) acts synergistically with copper (commonly found as a contaminant in Fe salts) to arrest growth in cells which were growing photoheterotrophically on acetate. Our results further show that such efflux proteins are not only required for a short-term response but continue to be highly expressed even after several transfers on Fe(II) and when the cells are using Fe(II) for growth. Our results also show that high Fe(II) concentrations cause the cells to reduce the number of transporters for siderophores or Fe(II). Together, the increase in efflux proteins alongside the decrease in proteins for iron influx clearly show the two aspects involved in managing intracellular metal concentrations, where cells must select a suitable and tolerable balance of influx and efflux. This is consistent with the observed decrease in abundance of the ferric uptake regulator (Fur), a master regulator of the iron response in a huge diversity of bacteria.

On first glance, this appears to be exactly what would be expected from the action of well-characterized iron response regulators. However, this response becomes more intriguing when we appreciate that almost everything known about iron homeostasis in bacteria comes from cells grown under oxic conditions, where iron toxicity is observed at much lower concentrations (38). Only a few studies have investigated iron stress under anoxic conditions, where bacteria can tolerate much higher iron concentrations in the millimolar range (25). It has been proposed that under such conditions, stress results from the formation of glutathione radicals (28) and reactive oxygen species by oxygen-independent photochemical reactions with Fe minerals (30, 31). However, we see no evidence of an oxidative stress response in Fe(II)-grown cells that might be consistent with this. Furthermore, minerals formed during Fe(II) oxidation are often observed to precipitate in the periplasm or on the cell surface in other metabolic types of Fe(II) oxidizers, but this is not observed in phototrophic Fe(II)-oxidizing bacteria. The reasons for the lack of encrustation are not fully resolved, but we may reasonably expect that the potential for encrustation would lead to an adaptive response involving changes in cell membrane structure; however, there is no strong evidence for this in our proteome data. Additionally, the formation of iron minerals which readily sorb nutrients, such as phosphorus, can remove essential nutrients from the growth media; however, we see no evidence for phosphorus limitation in the proteome of Fe(II)-grown cells. Indeed, despite the fact that Fe(II) oxidation is regarded as a novel metabolism which will induce numerous stresses, Fe(II)-grown cells do not

differ drastically from cells grown autotrophically with hydrogen. We would suggest that the only adaptations required by anoxygenic phototrophic Fe(II) oxidizers to thrive at these very high Fe(II) concentrations is a mechanism of Fe(II) oxidation and a typical suite of proteins for regulation of intracellular metal concentrations. The main challenge associated with utilizing Fe(II) as an electron donor, in our opinion, comes from the need to obtain all the carbon needed to build biomass solely from CO_2.

In addition to invoking a proteome response geared toward iron homeostasis, Fe(II)-grown cells show increased abundance of a number of key proteins in the photosynthetic electron transport chain. This is somewhat contradictory to our observation of short photosynthetic membranes and low abundance of pigment synthesis proteins under photoautotrophic conditions. One such protein is cytochrome c_2, which is a soluble high-potential iron-sulfur protein essential for photosynthesis. Its main function is in cyclic electron transfer for photosynthetic energy generation by shuttling electrons from the cytochrome bc_1 complex to the reaction center (33). Three proteins involved in proton transport across the membrane are also increased, with two subunits of the ATP synthase, and HppA, a pyrophosphate-energized proton pump. In addition to these are additional cytochromes (a cbb_3-type cytochrome *c* oxidase, cytochrome *b*, and cytochrome B561) and two photosynthetic reaction center subunits. Proteins involved in electron transport typically contain iron in their redox centers and are subsequently often shown to be downregulated as part of an iron-sparing response during iron limitation (39). A higher abundance of such proteins may suggest that the opposite strategy is employed under iron excess, such that iron is built into biomass as an attempt to reduce free iron within the cell.

Proton pumps, such as the F-type ATPases, and inorganic H^+ pyrophosphatases, such as HppA, which we observe to be upregulated, are also known to have a role in pH homeostasis by maintaining the optimum pH gradient between the intracellular and extracellular environments. Changes in pH occur during Fe(II) oxidation due to the production of protons (equation 1). This can lead to a low-pH microenvironment around anoxygenic phototrophic cells during Fe(II) oxidation and may be involved in the avoidance of Fe(III) mineral encrustation (22). While it is still to be determined whether such a pH management is passive or active, these provide promising targets for the investigation of pH homeostasis during Fe(II) oxidation.

Implications for detection of anoxygenic phototrophic Fe(II) oxidation in complex communities. One challenge which currently hinders the study of Fe(II) oxidation by anoxygenic phototrophs in the environment is the lack of general markers for this process. Some of the proteins thought to be associated with Fe(II) oxidation in this organism are detected under both photoautotrophic conditions. Jiao and Newman (18) established that proteins encoded by the *pio* operon are essential for this process. These consist of PioA (a periplasmic decaheme cytochrome), PioB (an outer membrane porin), and PioC (a periplasmic high-potential iron-sulfur cluster protein). PioAB is higher in abundance during growth on both Fe(II) and H_2 than on acetate in our study, whereas PioC shows no significant differential abundance between conditions. This is consistent with the results of Bose and Newman (32), who observed that *pioABC* is expressed under all photoautotrophic conditions they tested, yet its deletion only appears to be problematic in the case of growth on Fe(II). This result highlights the difficulties surrounding the detection of Fe(II) oxidation in the environment. The expression of the *pio* operon may give us a clue that photoautotrophy is the dominant metabolism in an environmental sample including *Rhodopseudomonas palustris* TIE-1, but it is not an indicator of Fe(II) oxidation. An alternative method to recognize photoautotrophy would, however, be useful, as our results show that the expression of carbon fixation pathways is not an indicator of photoautotrophy, as this is not overrepresented under any condition. The use of proteomics to create metabolic profiles for each substrate may provide an alternative route for determining the dominant metabolism in a complex environment. Based on this study, we could suggest that an Fe(II) oxidation-dominated system would be characterized by high *pio* gene expression with small intracellular membranes, coupled with high expression of efflux proteins and low

expression of siderophores. However, it must still be determined how these profiles are influenced by substrate concentrations, or by the presence of multiple substrates simultaneously, before proteomics could be confidently used to detect Fe(II) oxidation in the environment.

Conclusions. Our results show that each substrate utilized by the metabolically versatile *Rhodopseudomonas palustris* TIE-1 [Fe(II), H_2, or acetate] gives rise to a unique set of proteins. The main difference between conditions is driven by differences in carbon source, not because of altered abundance of proteins related to carbon metabolism, but because of lower growth rates with an inorganic carbon source. This may be related to difficulties in producing photosynthetic machinery from inorganic carbon sources. The response of the cells grown with very high concentrations of Fe(II) is consistent with well-characterized mechanisms for the management of iron homeostasis and shows no evidence for associated oxidative stress responses or unusual mechanisms of defense. This leads us to conclude that Fe(II) oxidation need not be considered a very specialized metabolism, so long as a mechanism of Fe(II) oxidation and some ability to control intracellular iron levels are present.

Many open questions remain to be answered in order to fully understand the adaptations anoxygenic phototrophic Fe(II) oxidizers implement to utilize these different substrates and to predict and detect which metabolism will be dominant in a given environment. Detailed understanding of the adaptation of anoxygenic phototrophic Fe(II) oxidizers to Fe(II) oxidation will require elucidation of the mechanisms by which iron is sensed and regulated in these cells. We must also know whether the proteome profile which arises during adaptation to Fe(II) is similar among all phototrophs or whether each species has a unique adaptation method. Second, to determine the dominant metabolism at play in a given environment, we must gain a better understanding of substrate preference and proteome adaptation when multiple substrates are available simultaneously, particularly at low concentrations more relevant to environmental systems. In tackling these problems, we may eventually be able to reach the ultimate goal of directly determining metabolic type and thus its role in biogeochemical cycling in complex natural environments.

MATERIALS AND METHODS

Bacterial growth conditions. Basal medium was prepared according to Jiao et al. (9), which included the addition of 1 ml per liter trace element solution, 1 ml per liter vitamin B_{12} solution, and 10 ml/liter of an altered vitamin solution (10), which contained 50 mg per liter riboflavin (17).

All experiments were conducted in 50-ml serum bottles with 25 ml medium and a headspace of either 90:10 N_2-CO_2 [for growth on acetate or Fe(II) experiments] or 80:20 H_2-CO_2 (for growth on H_2). For iron experiments, 10 mM $FeCl_2$ was added, and for acetate experiments, 10 mM sodium acetate (CH_3COONa) was added. In H_2 experiments, the headspace was exchanged every 2 to 3 days. Experiments were inoculated with 10% of an early stationary-phase preculture and placed approximately 30 cm from a 40 W halogen light bulb at 21°C. *Rhodopseudomonas palustris* TIE-1 cells are routinely maintained in our culture collection on Fe(II). Prior to the experiment, this stock culture was transferred on the chosen substrate a minimum of 6 times before the proteomics experiment. For the proteomics analysis, triplicate experiments for each substrate were conducted. Optical density, as a proxy for cell density, in H_2- and acetate-grown cultures was monitored by the transfer of 100 μl of culture to 96-well plates prior to the measurement of absorbance at 660 nm (Spekol 1300; Analytik Jena). Fe(II) oxidation was monitored using the ferrozine assay following fixation in 1 M HCl (1:10 sample/HCl). Cells were harvested in the mid-exponential phase when H_2 cultures reached an optical density at 660 nm (OD_{660}) of 0.38 to 0.43, acetate cultures reached an OD_{660} of 0.25 to 0.3, and Fe(II) cultures had a remaining concentration of 2.9 to 4.6 mM Fe(II) (where 10 mM was originally added). At the time of harvest, 20 ml of culture from each serum bottle was centrifuged at 7,000 rpm (5,752 $\times$ *g*) and 4°C for 30 min. Cell pellets were immediately frozen at −20°C until protein extraction.

Protein extraction and quantification. Frozen cell pellets were dissolved in an SDS protein extraction buffer containing 4% (wt/vol) SDS, 10 mM Tris-HCl (pH 8.0), 5 mM glycerol-2-phosphate, 5 mM sodium fluoride, 5 mM sodium orthovanadate, and 10 mM EDTA (pH 8.0). This solution was incubated at 95°C for 10 min and then placed in a sonicating bath, on a moderate setting, for 2 min. For the reduction of cysteine disulfide bonds, dithiothreitol was added to a final concentration of 10 mM. Alkylation of the reduced cysteine bonds was achieved by the addition of 5.5 mM iodoacetamide and shaking (650 rpm) for 45 min at room temperature in the dark. Nonsoluble cell debris was pelleted by centrifugation at 7,000 rpm (5,752 $\times$ *g*) and 4°C for 10 min.

Proteins were precipitated by mixing the supernatant with eight sample volumes of ice-cold acetone and one sample volume of ice-cold methanol. The mixture was vortexed and incubated at −20°C

overnight. The precipitated proteins were centrifuged at 1,000 rpm (117 × *g*) for 5 min, and the pellet washed 3 times with ice-cold acetone. After the final wash step, the pellet was air-dried at room temperature.

Protein quantification and data analysis. The protein pellet was rehydrated in urea buffer containing 6 M urea and 2 M thiourea in 100 mM Tris-HCl (pH 7.5). Proteins (10 μg per condition) were purified on an SDS-PAGE gel, and Coomassie-stained gel pieces were digested in gel with trypsin, as described previously (40). After desalting using C_{18} Stage Tips (41), extracted peptides were separated on an EasyLC nano-high-performance liquid chromatograph (HPLC; Thermo Scientific) coupled to an LTQ Orbitrap XL (Thermo Scientific), as described elsewhere (42), with slight modifications: the peptide mixtures were injected onto the column in HPLC solvent A (0.1% formic acid) at a flow rate of 500 nl/min and subsequently eluted with a 227-min segmented gradient of 5:33:50:90% of HPLC solvent B (80% acetonitrile in 0.1% formic acid) at a flow rate of 200 nl/min.

Precursor ions were acquired in the mass range from *m/z* 300 to 2,000 in the Orbitrap mass analyzer at a resolution of 60,000. An accumulation target value of 10^6 charges was set, and the lock mass option was used for internal calibration (43). The 10 most intense ions were sequentially isolated and fragmented in the linear ion trap using collision-induced dissociation (CID) at the ion accumulation target value of 5,000 and default CID settings. Sequenced precursor masses were excluded from further selection for 90 s.

The acquired MS spectra were processed with the MaxQuant software package version 1.5.2.8 (44) with the integrated Andromeda search engine (45). The database search was performed against a target-decoy *Rhodopseudomonas palustris* TIE-1 database obtained from UniProt, containing 5,247 protein entries, and 285 commonly observed contaminants. Endoprotease trypsin was defined as protease with a maximum of two missed cleavages. Oxidation of methionine and N-terminal acetylation were specified as variable modifications, whereas carbamidomethylation on cysteine was set as a fixed modification. Initial maximum allowed mass tolerance was set to 4.5 ppm (for the survey scan) and 0.5 Da for CID fragment ions. Peptide, protein, and modification site identifications were reported at a false-discovery rate (FDR) of 0.01, estimated by the target-decoy approach (46). The label-free algorithm was enabled, as was the "match between runs" option (47).

Downstream analysis and functional interpretation. Downstream analysis was performed in the R environment (48). The resultant proteome profiles obtained were quality checked for replicate correlation using principal component analysis and hierarchical clustering. The data were then filtered for low-abundance proteins via a two-step process. First, all proteins were ranked (in descending order) by label-free quantification (LFQ) intensity, and the 3rd quartile LFQ value was set as the minimum intensity threshold. Second, to pass the filtering, all samples within a condition must have an LFQ intensity above this threshold. Contaminants and reverse hits were also removed from downstream analyses. Following low-abundance filtering, the LFQ values were quantile normalized (a common global adjustment method that assumes that the statistical distribution of each sample is the same) using the MSnbase package (49). Similarity between replicates and between different conditions was calculated by taking the average of the Spearman correlation calculated for each possible comparison (between triplicates, $n = 3$; between conditions, $n = 9$). In order to statistically compare protein abundances across conditions (even when the protein was not detected under one of the conditions), imputation was used on the data using a mixed model of nearest-neighbor averaging and left-censored missing data from a truncated distribution (49). Comparisons in which both conditions contained imputed values were removed. Proteins which were significantly different between conditions were identified using analysis of variance (ANOVA), followed by the Tukey *post hoc* test. Significance was set at an adjusted *P* value of 0.05 following Benjamini-Hochberg multiple-correction testing. Functional information, namely, gene ontology (GO) and KEGG orthology (KO), for *Rhodopseudomonas palustris* TIE-1 proteins was retrieved using the UniProt.ws package (50). Overrepresentation testing for GO and KO was done for each comparison via the clusterProfiler package based on hypergeometric distribution (adjusted $P \leq 0.05$) (51).

Cryogenic transmission electron microscopy. In order to observe visual differences in cell structure and morphology in cells grown on each of the three substrates, we used cryogenic transmission electron microscopy (cryo-TEM). TEM allows for investigation of the internal structure of cells and, when coupled to cryogenic sample preparation, allows observation of the cells in their hydrated state. For cells grown on H_2 or acetate, 1 ml of culture was removed from cultures prepared to different growth stages representative of early exponential growth, late-exponential growth, and stationary phase. The OD_{660} was measured before the cells were pelleted by centrifugation (room temperature, 6,000 rpm [4,226 × *g*], 10 min), and resuspended in Milli-Q (MQ) H_2O to remove any salts which would interfere with the analysis. Some samples, especially from the early phase cultures where low cell numbers were present, were concentrated by centrifugation at this step. For cells grown with Fe(II), 1 ml of sample was removed in an anoxic glove box and centrifuged to pellet the cells before resuspending the cell pellet in anoxic MQ H_2O. To quantify the extent of iron oxidation which had occurred in these cultures, 100 μl of sample was extracted in 900 μl of 1 M HCl, and the Fe(II) concentration was measured using the ferrozine assay (53). Samples were processed for subsequent analysis as quickly as possible after removal from the glove box.

For cryo-TEM analysis, 4 μl of sample was added onto a Cu-holey carbon (300 mesh) grid (Agar Scientific Ltd., Essex, England). Blotting paper was lightly touched onto the front side of the sample to remove excess water immediately prior to vitrification by flash-freezing in liquid ethane (around −183°C). This plunge-freezing protocol results in a very thin layer of ice, where the vast majority of cells lie flat against the grid. Samples were transferred into a cryo-holder (Gatan, Évry, France) and kept at liquid nitrogen temperature (around −196°C). Samples were inserted into a JEOL 2100 transmission electron microscope (TEM) equipped with an LaB_6 cathode working at an accelerating voltage of 200 kV. Images

were recorded under low-dose conditions (10 electrons per Å^2) at a nominal magnification ranging from ×5,000 to 40,000 (spatial resolution ranging from 485 to 3,883 pixels · μm^{-1}) using a 2 K-by-2 K charge-coupled device (CCD) camera (US 1000; Gatan). For acetate-grown cells, 69 images of cells were collected over 4 growth stages. For iron-grown cells, 71 images were collected across 5 growth stages. For hydrogen-grown cells, 102 images were collected over 4 growth stages. The contrast and brightness of the images presented in Fig. 3 were adjusted slightly in ImageJ. To compare the sizes of the intracellular membranes, images were selected in which the entire cell was contained within the image and in which the intracellular membranes (or lack thereof) were easily distinguishable. As no difference between different growth phases was observed, samples from all stages were counted together in this analysis. The area covered by the intracellular membrane was measured manually using ImageJ. For cells in which membranes appeared on both sides of the cell, the measurement for each side was combined to provide the total area of the cell covered by intracellular membrane. The length of the cells was also measured manually in ImageJ, with no significant differences observed.

Data availability. The mass spectrometry proteomics data have been deposited with the ProteomeXchange Consortium via the PRIDE (52) partner repository under the data set identifier PXD009629 (http://proteomecentral.proteomexchange.org/cgi/GetDataset?ID=PXD009629).

SUPPLEMENTAL MATERIAL

Supplemental material for this article may be found at https://doi.org/10.1128/AEM.01166-18.

SUPPLEMENTAL FILE 1, PDF file, 0.4 MB.

SUPPLEMENTAL FILE 2, XLSX file, 0.2 MB.

ACKNOWLEDGMENTS

We sincerely thank Dianne Newman and Gargi Kulkarni (California Institute of Technology) for their valuable input on the interpretation of the proteomics data and for helpful comments on the manuscript. We also thank Silke Wahl (University of Tübingen) for assistance with protein digests, Jean-Michel Guigner (IMPMC) for operation and sample prep during cryo-TEM, and the Tübingen Geomicrobiology group for their consistent input and support.

Casey Bryce and Andreas Kappler were funded by the European Research Council (ERC) under grant 307320-MICROFOX. Sara Kleindienst is funded by an Emmy-Noether fellowship (grant 326028733) from the German Research Foundation (Deutsche Forschungsgemeinschaft [DFG]).

We declare no conflicts of interest.

REFERENCES

1. Konhauser KO, Hamade T, Raiswell R, Morris RC, Ferris FG, Southam G, Canfield DE. 2002. Could bacteria have formed the Precambrian banded iron formations? Geology 30:1079–1082. https://doi.org/10.1130/0091-7613(2002)030<1079:CBHFTP>2.0.CO;2.
2. Posth NR, Konhauser KO, Kappler A. 2013. Microbiological processes in banded iron formation deposition. Sedimentology 60:1733–1754. https://doi.org/10.1111/sed.12051.
3. Kappler A, Newman DK. 2005. Deposition of banded iron formations by anoxygenic phototrophic Fe(II)-oxidizing bacteria. Geology 33:865–868. https://doi.org/10.1130/G21658.1.
4. Lliros M, Garcia-Armisen T, Darchambeau F, Morana C, Triadó-Margarit X, Inceoğlu Ö, Borrego CM, Bouillon S, Servais P, Borges AV, Descy J, Canfield DE, Crowe SA. 2015. Pelagic photoferrotrophy and iron cycling in a modern ferruginous basin. Sci Rep 5:13803. https://doi.org/10.1038/srep13803.
5. Crowe SA, Jones C, Katsev S, Magen C, O'Neill AH, Sturm A, Canfield DE, Haffner GD, Mucci A, Sundby B, Fowle DA. 2008. Photoferrotrophs thrive in an Archean Ocean analogue. Proc Natl Acad Sci U S A 105:15938–15943. https://doi.org/10.1073/pnas.0805313105.
6. Crowe S, Hahn A, Morgan-Lang C, Thompson K, Simister R, Lliros M, Hirst M, Hallam S. 2017. Draft genome sequence of the pelagic photoferrotroph Chlorobium phaeoferrooxidans. Genome Announc 5:e01584-16. https://doi.org/10.1128/genomeA.01584-16.
7. Walter XA, Picazo A, Miracle MR, Vicente E, Camacho A, Aragno M, Zopfi J. 2014. Phototrophic Fe(II)-oxidation in the chemocline of a ferruginous meromictic lake. Front Microbiol 5:713. https://doi.org/10.3389/fmicb.2014.00713.
8. Berg JS, Michellod D, Pjevac P, Martinez-Perez C, Buckner CRT, Hach PF, Schubert CJ, Milucka J, Kuypers MMM. 2016. Intensive cryptic microbial iron cycling in the low iron water column of the meromictic Lake Cadagno. Environ Microbiol 18:5288–5302. https://doi.org/10.1111/1462-2920.13587.
9. Jiao Y, Kappler A, Croal LR, Newman K, Newman DK. 2005. Isolation and characterization of a genetically tractable photoautotrophic Fe(II)-oxidizing bacterium, Rhodopseudomonas palustris strain TIE-1. Appl Environ Microbiol 71:4487–4496. https://doi.org/10.1128/AEM.71.8.4487-4496.2005.
10. Ehrenreich A, Widdel F. 1994. Anaerobic oxidation of ferrous iron by purple bacteria, a new type of phototrophic metabolism. Appl Environ Microbiol 60:4517–4526.
11. Laufer K, Nordhoff M, Schmidt C, Behrens S, Jørgensen BB, Kappler A. 2016. Coexistence of microaerophilic, nitrate-reducing, and phototrophic Fe(II) oxidizers and Fe(III) reducers in coastal marine sediment. Appl Environ Microbiol 82:1433–1447. https://doi.org/10.1128/AEM.03527-15.
12. Laufer K, Niemeyer A, Nikeleit V, Halama M, Byrne JM, Kappler A. 2017. Physiological characterization of a halotolerant anoxygenic phototrophic Fe(II)-oxidizing green-sulfur bacterium isolated from a marine sediment. FEMS Microbiol Ecol 93:fix054. https://doi.org/10.1093/femsec/fix054.
13. Wu W, Swanner ED, Hao L, Zeitvogel F, Obst M, Pan Y, Kappler A. 2014. Characterization of the physiology and cell-mineral interactions of the marine anoxygenic phototrophic Fe(II) oxidizer Rhodovulum iodosum–implications for Precambrian Fe(II) oxidation. FEMS Microbiol Ecol 88:503–515. https://doi.org/10.1111/1574-6941.12315.
14. Straub KL, Raineyr FA, Widdell F. 1999. Rhodovulum iodosum sp. nov.

and Rhodovulum robiginosum sp. nov., two new marine phototrophic ferrous-iron-oxidizing purple bacteria. Int J Syst Biotechnol 49:729–735.
15. Thompson KJ, Simister RL, Hahn AS, Hallam SJ, Crowe SA, Field E. 2017. Nutrient acquisition and the metabolic potential of photoferrotrophic chlorobi. Front Microbiol 8:1–16. https://doi.org/10.3389/fmicb.2017.01212.
16. Croal LR, Jiao Y, Kappler A, Newman DK. 2009. Phototrophic Fe(II) oxidation in an atmosphere of H_2: implications for archean banded iron formations. Geobiology 7:21–24. https://doi.org/10.1111/j.1472-4669.2008.00185.x.
17. Melton ED, Schmidt C, Behrens S, Schink B, Kappler A. 2014. Metabolic flexibility and substrate preference by the Fe(II)-oxidizing purple nonsulphur bacterium Rhodopseudomonas palustris strain TIE-1. Geomicrobiol J 31:37–41. https://doi.org/10.1080/01490451.2014.901439.
18. Jiao Y, Newman DK. 2007. The *pio* operon is essential for phototrophic Fe(II) oxidation in *Rhodopseudomonas palustris* TIE-1. J Bacteriol 189:1765–1773. https://doi.org/10.1128/JB.00776-06.
19. Shi L, Dong H, Reguera G, Beyenal H, Lu A, Liu J, Yu H-Q, Fredrickson JK. 2016. Extracellular electron transfer mechanisms between microorganisms and minerals. Nat Rev Microbiol 14:651–662. https://doi.org/10.1038/nrmicro.2016.93.
20. Croal LR, Jiao Y, Newman DK. 2007. The *fox* operon from *Rhodobacter* strain SW2 promotes phototrophic Fe(II) oxidation in *Rhodobacter capsulatus* SB1003. J Bacteriol 189:1774–1782. https://doi.org/10.1128/JB.01395-06.
21. Pereira L, Saraiva IH, So A, Oliveira F, Soares CM, Louro RO, Frazão C. 2017. Molecular structure of FoxE, the putative iron oxidase of Rhodobacter ferrooxidans SW2. Biochim Biophys Acta 1858:847–853. https://doi.org/10.1016/j.bbabio.2017.07.002.
22. Hegler F, Schmidt C, Schwarz H, Kappler A. 2010. Does a low-pH microenvironment around phototrophic FeII-oxidizing bacteria prevent cell encrustation by FeIII minerals? FEMS Microbiol Ecol 74:592–600. https://doi.org/10.1111/j.1574-6941.2010.00975.x.
23. Miot J, Benzerara K, Obst M, Kappler A, Hegler F, Schädler S, Bouchez C, Guyot F, Morin G. 2009. Extracellular iron biomineralization by photoautotrophic iron-oxidizing bacteria. Appl Environ Microbiol 75:5586–5591. https://doi.org/10.1128/AEM.00490-09.
24. Eickhoff M, Obst M, Schröder C, Hitchcock AP, Tyliszczak T, Martinez RE, Robbins LJ, Konhauser KO, Kappler A. 2014. Nickel partitioning in biogenic and abiogenic ferrihydrite: the influence of silica and implications for ancient environments. Geochim Cosmochim Acta 140:65–79. https://doi.org/10.1016/j.gca.2014.05.021.
25. Poulain AJ, Newman DK. 2009. Rhodobacter capsulatus catalyzes light-dependent Fe(II) oxidation under anaerobic conditions as a potential detoxification mechanism. Appl Environ Microbiol 75:6639–6646. https://doi.org/10.1128/AEM.00054-09.
26. Bird LJ, Coleman ML, Newman DK. 2013. Iron and copper act synergistically to delay anaerobic growth of bacteria. Appl Environ Microbiol 79:3619–3627. https://doi.org/10.1128/AEM.03944-12.
27. Kreamer NN, Costa F, Newman K. 2015. The ferrous iron-responsive BqsRS two-component system. mBio 6:e02549-14. https://doi.org/10.1128/mBio.02549-14.
28. Dunning JC, Ma Y, Marquis RE. 1998. Anaerobic killing of oral streptococci by reduced, transition metal cations. Appl Environ Microbiol 64:27–33.
29. Touati D. 2000. Iron and oxidative stress in bacteria. Arch Biochem Biophys 373:1–6. https://doi.org/10.1006/abbi.1999.1518.
30. Gauger T, Byrne JM, Konhauser KO, Obst M, Crowe S, Kappler A. 2016. Influence of organics and silica on Fe(II) oxidation rates and cell-mineral aggregate formation by the green-sulfur Fe(II)-oxidizing bacterium Chlorobium ferrooxidans KoFox–implications for Fe(II) oxidation in ancient oceans. Earth Planet Sci Lett 443:81–89. https://doi.org/10.1016/j.epsl.2016.03.022.
31. Borda M, ELsetinow AR, Strongin DR, Schoonen M. 2003. A mechanism for the production of hydroxyl radical at surface defect sites on pyrite. Geochim Cosmochim Acta 67:935–939. https://doi.org/10.1016/S0016-7037(02)01222-X.
32. Bose A, Newman DK. 2011. Regulation of the phototrophic iron oxidation (*pio*) genes in *Rhodopseudomonas palustris* TIE-1 is mediated by the global regulator, FixK. Mol Microbiol 79:63–75. https://doi.org/10.1111/j.1365-2958.2010.07430.x.
33. Bird L, Saraiva I, Park S, Calcada E, Salgueiro C, Nitschke W, Louro R, Newman D. 2014. Nonredundant roles for cytochrome c_2 and two high-potential iron-sulfur proteins in the photoferrotroph *Rhodopseudomonas palustris* TIE-1. J Bacteriol 196:850–858. https://doi.org/10.1128/JB.00843-13.
34. McKinlay JB, Harwood CS. 2010. Carbon dioxide fixation as a central redox cofactor recycling mechanism in bacteria. Proc Natl Acad Sci U S A 107:11669–11675. https://doi.org/10.1073/pnas.1006175107.
35. Yang J, Yin L, Lessner FH, Nakayasu ES, Payne SH, Fixen KR, Gallagher L, Harwood CS. 2017. Genes essential for phototrophic growth by a purple alphaproteobacterium. Environ Microbiol 19:3567–3578. https://doi.org/10.1111/1462-2920.13852.
36. Niederman RA. 2013. Membrane development in purple photosynthetic bacteria in response to alterations in light intensity and oxygen tension. Photosynth Res 116:333–348. https://doi.org/10.1007/s11120-013-9851-0.
37. Varga A, Staehelin LA. 1983. Spatial differentiation in photosynthetic and non-photosynthetic membranes of Rhodopseudomonas palustris. J Bacteriol 154:1414–1430.
38. Frawley E, Fang F. 2014. The ins and outs of bacterial iron metabolism. Mol Microbiol 93:609–616. https://doi.org/10.1111/mmi.12709.
39. Meibom KL, Cabello EM, Bernier-Latmani R. 2018. The small RNA RyhB is a regulator of cytochrome expression in *Shewanella oneidensis*. Front Microbiol 9:268. https://doi.org/10.3389/fmicb.2018.00268.
40. Borchert N, Dieterich C, Krug K, Schütz W, Jung S, Nordheim A, Sommer R, Macek B. 2010. Proteogenomics of Pristionchus pacificus reveals distinct proteome structure of nematode models. Genome Res 20:837–846. https://doi.org/10.1101/gr.103119.109.
41. Rappsilber J, Mann M, Ishihama Y. 2007. Protocol for micro-purification, enrichment, pre-fractionation and storage of peptides for proteomics using StageTips. Nat Protoc 2:1896–1906. https://doi.org/10.1038/nprot.2007.261.
42. Franz-Wachtel M, Eisler S, Krug K, Wahl S, Carpy A, Nordheim A, Pfizenmaier K, Hausser A, Macek B. 2012. Global detection of protein kinase D-dependent phosphorylation events in nocodazole-treated human cells. Mol Cell Proteomics 11:160–170. https://doi.org/10.1074/mcp.M111.016014.
43. Olsen J, de Godoy L, Li G, Macek B, Mortensen P, Pesch R, Makarov A, Lange O, Horning S, Mann M. 2005. Parts per million mass accuracy on an Orbitrap mass spectrometer via lock mass injection into a C-trap. Mol Cell Proteomics 4:2010–2021. https://doi.org/10.1074/mcp.T500030-MCP200.
44. Cox J, Mann M. 2008. MaxQuant enables high peptide identification rates, individualized p.p.b.-range mass accuracies and proteome-wide protein quantification. Nat Biotechnol 26:1367–1372. https://doi.org/10.1038/nbt.1511.
45. Cox J, Neuhauser N, Michalski A, Scheltema R, Olsen J, Mann M. 2011. Andromeda: a peptide search engine integrated into the MaxQuant environment. J Proteome Res 10:1794–1805. https://doi.org/10.1021/pr101065j.
46. Elias J, Gygi S. 2007. Target-decoy search strategy for increased confidence in large-scale protein identifications by mass spectrometry. Nat Methods 4:207–214. https://doi.org/10.1038/nmeth1019.
47. Luber A, Cox J, Lauterbach H, Fancke B, Selbach M, Tschopp J, Akira S, Wiegand M, Hochrein H, O'Keeffe M, Mann M. 2010. Quantitative proteomics reveals subset-specific viral recognition in dendritic cells. Immunity 32:149–151. https://doi.org/10.1016/j.immuni.2010.02.006.
48. R Core Team. 2018. R: a language and environment for statistical computing. R Foundation for Statistical Computing, Vienna, Austria.
49. Gatto L, Lilley KS. 2012. MSnbase—an R/Bioconductor package for isobaric tagged mass spectrometry data visualization, processing and quantitation. Bioinformatics 28:288–289. https://doi.org/10.1093/bioinformatics/btr645.
50. Carlson M. 2017. UniProt.ws: R interface to UniProt web services. R package version 2.20.0. http://bioconductor.org/packages/release/bioc/html/UniProt.ws.html.
51. Yu G, Wang L-G, Han Y, He Q-Y. 2012. clusterProfiler: an R package for comparing biological themes among gene clusters. OMICS 16:284–287. https://doi.org/10.1089/omi.2011.0118.
52. Vizcaíno JA, Csordas A, Del-Toro N, Dianes JA, Griss J, Lavidas I, Mayer G, Perez-Riverol Y, Reisinger F, Ternent T, Xu QW, Wang R, Hermjakob H. 2016. 2016 update of the PRIDE database and its related tools. Nucleic Acids Res 44:D447–D456. https://doi.org/10.1093/nar/gkv1145.
53. Hegler F, Posth NR, Jiang J, Kappler A. 2008. Physiology of phototrophic iron(II)-oxidizing bacteria: implications for modern and ancient environments. FEMS Microbiol Ecol 66:250–260. https://doi.org/10.1111/j.1574-6941.2008.00592.x.